Biosensors and Bioelectronics 143 (2019) 111612

Contents lists available at ScienceDirect

Biosensors and Bioelectronics

journal homepage: www.elsevier.com/locate/bios

PtCu nanoprobe-initiated cascade reaction modulated iodide-responsive sensing interface for improved electrochemical immunosensor of neuron-specific enolase

Chi Zhang, Zhanfang Ma*

Department of Chemistry, Capital Normal University, Beijing, 100048, China

ARTICLE INFO

Keywords:
Improved electrochemical immunosensor
Cascade reaction
PtCu nanoparticles
Iodide-responsive sensing interface
Neuron-specific enolase

ABSTRACT

The method of transferring the immunoreaction from electrode surface to tube can greatly improve the analytical performance of electrochemical immunosensor. In this work, based on PtCu nanoprobe-mediated and iodide-catalyzed cascade reaction, an improved electrochemical immunosensor was elaborately designed for neuron-specific enolase (NSE) detection. PtCu nanoparticles combined with NSE antibody (Ab_2) were used as immunoprobes to trigger cascade reaction. With high catalytic activity towards the oxidation of iodide, PtCu nanoprobes catalyzed iodide to iodine in the presence of H_2O_2, leading to the decrease of iodide. Subsequently, as a bridge between the tube and iodide-responsive sensing interface, the residual iodide in tube was employed to catalyze the transition from thiol substances (RSH) to disulfide substances (RSSR) on electrode surface. On the basis of this property, thiol-modified DNA (DNA-SH) and 6-mercaptohexanol (MCH) reacted with H_2O_2 and the residual iodide to form disulfide substances and detach from the electrode surface, causing the decrease of interface resistance in different degrees. Then square wave voltammetry (SWV) was applied for current signal of electrochemical sensing interface to achieve the quantitative detection of NSE. Under optimal conditions, this improved biosensor demonstrated excellent selectivity, stability and reproducibility with wide linear range from 0.0001 to 100 ng mL^{-1} and ultralow detection limit of 52.14 fg mL^{-1} for NSE, thus holding great promise for sensitive determination of tumor markers.

1. Introduction

Cancer is the main cause of death worldwide (Wang and Ma, 2019; Yang et al., 2017). As people's bad living habits and increasingly severe environmental pollution, lung cancer with the highest mortality rate has become the most threatening cancer to human's health (Zhou et al., 2019). Among all cases of lung cancer, small cell lung cancer (SCLC) is one of the major subtypes, accounting for about 20% in various types of lung cancer (Yang et al., 2019). Currently, a series of approaches have been applied to the determination of SCLC, such as magnetic resonance imaging (MRI), positron emission tomography (PET), chest radiograph (CRG), computed tomography (CT) and biopsy. However, these methods not only require professional operators, large-scale instruments and the detectable diameter of tumor ($\geq$10 mm), but also take the risk of physical or chemical damage (Eisenhauer et al., 2009; Wang, 2017), which can restrict the early diagnosis of SCLC. In comparison with these methods, the quantitative detection of tumor markers has the advantages of less invasive procedures and high sensitivity (Yin and Ma, 2019; Zheng and Ma, 2019), which is of great importance for occurrence and progression of cancer (Ren et al. 2017, 2018). As the most reliable and sensitive biomarker of SCLC, neuron-specific enolase (NSE) is a specific predictor for early diagnosis and subsequent treatment of SCLC (Carney et al., 1982; Han et al., 2012). At present, lots of methods have been developed for determination of NSE, for example, surface-enhanced Raman scattering immunoassay (Gao et al., 2017), photoelectrochemical immunoassay (Li et al., 2017) and electrochemical immunoassay (Wang et al., 2018; Yin et al., 2018). Among these approaches, electrochemical immunoassay plays an irreplaceable role owing to its simple operation, ease of miniaturization and high sensitivity (Hou et al., 2014; Wei et al., 2017).

Electrochemical immunoassay mainly involves the immobilization of antibodies, antigen-antibody specific recognition and the combination of blocking reagent. For sandwich-type electrochemical immunosensor, immunoprobes are introduced to the sensing interface. Though electrochemical immunoassay has made great progress in the detection of tumor markers, there are still several inherent drawbacks

* Corresponding author.
E-mail address: mazhanfang@cnu.edu.cn (Z. Ma).

https://doi.org/10.1016/j.bios.2019.111612
Received 13 July 2019; Received in revised form 6 August 2019; Accepted 18 August 2019
Available online 22 August 2019
0956-5663/

that limit the analytical performance to some extent. First, because of the high impedance of antigen, antibody, blocking agent and immunoprobes, an insulating layer is generated on electrode (Zhang et al., 2018a; Liang et al., 2019), which hinders the interfacial electron transfer and decreases the signal response (Fan et al., 2014). Second, during the construction of biosensor, the incubation of complex fluids may cause non-specific adsorption of proteins on modified electrode (Riedel et al., 2013), resulting in non-specific response and degradation of analytical performance. In addition, electrochemical sensing interface may be easily contaminated owing to the complicated modification steps and multistep incubation process (Ko et al., 2014). Hence, given the problems above, it is urgent to seek more effective methods to solve these problems of electrochemical sensing interface.

In this work, an electrochemical immunosensor was improved by transferring the immunoreaction from electrode surface to tube. In addition, considering the high catalytic activity of PtCu nanoparticles (Li et al., 2018), multifunctionalized PtCu nanoparticles conjugated with NSE antibody (Ab_2) as nanoprobes can initiate cascade catalysis. Combining the PtCu nanoprobe-triggered cascade reaction with iodide-responsive sensing interface was employed to improve the performance of conventional electrochemical immunosensor for NSE detection. In this approach, PtCu nanoprobes catalyzed the oxidation of iodide to iodine, causing the consumption of iodide. After immunoreaction, the residual iodide in tube further catalyzed thiol-modified DNA (DNA-SH) and 6-mercaptohexanol (MCH) on the electrode surface to form disulfide substances. Then, DNA and MCH with poor conductivity (Wang et al., 2017; Zhao et al., 2019) was detached from the electrode surface after washing with phosphate buffer solution (PBS, pH = 7.4), leading to the decrease of interface resistance in different degrees to attain the sensitive detection of NSE. Compared with conventional electrochemical immunosensor, the improved one possessed lower interface resistance due to the transfer of immunoreaction from electrode surface to tube so that the current differences caused by target were improved effectively. In addition, the PtCu nanoprobe-initiated cascade reaction can effectively enhance the sensitivity of immunosensor because of the catalytic activity of PtCu nanoparticles and iodide. Furthermore, complicated modification steps and multistep incubation process on electrode surface were reduced significantly, which lowered the non-specific adsorption and lessened the contamination of sensing interface. Thus, the proposed immunosensor efficiently overcame the inherent drawbacks of electrochemical sensing interface and showed prominent analytical performance for NSE detection, offering the great potential applications in clinical diagnosis for sensitive detection of tumor markers.

2. Experimental

2.1. Materials and reagents

Neuron-specific enolase (NSE), carcinoembryonic antigen (CEA), prostate specific antigen (PSA), carbohydrate antigen 24-2 (CA24-2), carbohydrate antigen 19-9 (CA19-9) and NSE antibodies (Ab_1, Ab_2) were provided by Shanghai LincBio Science Co., Ltd (Shanghai, China). The sequence of thiol-modified DNA (DNA-SH) was listed in Table S1. Tris(2-carboxyethyl) phosphine hydrochloride (TCEP), (N-hydroxysuccinimide) (NHS), (1-ethyl-3-[3-dimethylaminopropyl] carbodiimide hydrochloride) (EDC), 6-mercaptohexanol (MCH) and hexaammineruthenium(III) chloride (RuHex) were provided by Sigma-aldrich (Beijing, China). Carboxyl group modified magnetic microbeads (MBs, 5 mg mL^{-1}) were obtained from Tianjin BaseLine ChromTech Research Centre (Tianjin, China). Cetyltrimethylammonium chloride (CTAC), oleylamine (OAm), $Pt(acac)_2$, $CuCl_2{\cdot}H_2O$ and diglycolamine (DGA) were supplied from Aladdin Chemical Reagent Company (Shanghai, China). Hydrogen peroxide (H_2O_2) was bought from Alfa Aesar (Tianjin, China). Sodium iodide was provided by Tianjin Fuchen Chemical Reagent Co., Ltd (Tianjin, China). $HAuCl_4{\cdot}3H_2O$ was obtained from Alfa Aesar (Tianjin, China). Ultrapure water (resistivity = 18.25 MΩ cm) was used to prepare the aqueous solution.

2.2. Apparatus

The morphologies of samples were recorded by high-resolution transmission electron microscopy (HRTEM, JEM-2100F) and scanning electron microscope (SEM, HITACHI S-4800). The elements and components were analyzed by using X-ray photoelectron spectroscopy (XPS, ESCALAB 250) and energy disperse spectroscopy (EDS, HITACHI S-4800 and JEM-2100F). The catalytic activity was investigated by using UV-2550 UV–vis spectrophotometer (Shimadzu, Japan).

All electrochemical measurements were operated on CHI600e electrochemical workstation (Chenhua Instruments Co., Shanghai, China). A three-electrode system was consist of a saturated Ag/AgCl electrode or calomel electrode as reference electrode, a platinum wire and a modified glassy carbon electrode (GCE, Φ = 4 mm) as counter electrode and working electrode, respectively.

2.3. Synthesis of Ab_1-functionalized magnetic beads

Firstly, 1 mL carboxyl group (-COOH) modified magnetic beads (MBs) were washed with water carefully. Then, the mixed solution of NHS (0.1 M) and EDC (0.4 M) was added into MBs to activate -COOH for 0.5 h at 37 °C. After washing three times with water, 1 mL NSE antibody (Ab_1, 200 μg mL^{-1}) was added to incubate for 3 h, forming the complex of Ab_1-MBs. In order to avoid non-specific absorption, Ab_1-MBs were incubated with bovine serum albumin (BSA, 1%) for 0.5 h. Finally, the product was washed carefully and re-dispersed as solution with 1 mL water.

2.4. Preparation of Ab_2-functionalized PtCu nanoprobes

PtCu nanoparticles were prepared in accordance with the published literature (Niu et al., 2019). 0.28 g CTAC was dissolved into 35 mL oleylamine (OAm) and the mixture became a homogeneous solution after ultrasound 30 min. After that, 0.012 g $CuCl_2{\cdot}2H_2O$, 0.028 g $Pt(acac)_2$ and 87.6 μL diglycolamine (DGA) were mixed together into the above solution. After ultrasound another 20 min, the mixture turned a uniform blue-green. Then, it can be transferred into 40 mL Teflon-lined stainless autoclave and maintain 180 °C for 10 h. After natural cooling, the product was centrifuged (6000 rpm, 5 min) and washed with the mixture of cyclohexane and ethanol, then re-dispersed as solution for later use. Next, 100 μL NSE antibody (Ab_2, 1 mg mL^{-1}) was mixed with 1 mL PtCu nanoparticles (1 mg mL^{-1}) and incubated overnight. 1% BSA was used for preventing non-specific binding sites. Finally, Ab_2-functionalized PtCu nanoprobes were collected by centrifugation, dispersed as solution and kept 4 °C in a refrigerator.

2.5. Fabrication of electrochemical sensing interface

A GCE was polished with Al_2O_3 powder (0.05 μm) carefully. Then, after washing with water and ethanol by sonication, Au nanoparticles were electrodeposited on glassy carbon electrode in 5 mM $HAuCl_4$ solution at −0.2 V for 60 s (Zhao and Ma, 2017). Pretreated with TCEP (100 μM) for 1 h, DNA-SH (20 μL, 1 μM) was incubated on modified electrode overnight at 37 °C. After that, MCH (20 μL, 1 mM) was incubated on electrode for another 1 h at ambient temperature. Then, the electrode (MCH/DNA-SH/Au/GCE) was rinsed with PBS (pH = 7.4) carefully so as to obtain DNA-SH and MCH modified electrode as the iodide-responsive sensing interface.

2.6. Immunoreaction in the tube

Firstly, 30 μL Ab_1-MBs was transferred into a tube. After magnetic separation, a series of NSE standard solutions were added to incubate

with Ab_1-MBs for 40 min at 37 °C. Then, the product was washed thoroughly by magnetic separation. After that, 30 μL as-prepared Ab_2-PtCu immunoprobes were incubated with NSE/Ab_1-MBs for 50 min at 37 °C. And the sandwich-type bioconjugate (Ab_2-PtCu/NSE/Ab_1-MBs) was obtained by magnetic separation after washing with water. Subsequently, sodium iodide (400 μM) and H_2O_2 (400 μM) were added into tube and the mixture reacted for 1 h at 37 °C.

2.7. Electrochemical detection of NSE

The mixture containing H_2O_2 (100 μM) and the residual solution after immunoreaction was incubated on the surface of electrode (MCH/DNA-SH/Au/GCE) to react for 50 min at 37 °C. After thoroughly rinsing with PBS (pH = 7.4), the current signals of square wave voltammetry were determined in 0.01 M PBS (pH = 7.4) containing 5 mM $[Fe(CN)_6]^{3-/4-}$ at −0.2 − 0.8 V (vs. Ag/AgCl).

3. Results and discussion

3.1. Principle of the biosensor

The principle and stepwise modification process of the immunosensor were depicted in Scheme 1. The immune process and electrochemical detection were respectively implemented in tube and on electrode surface. First of all, gold nanoparticles as the substrate were electrodeposited on electrode, which can be used to immobilize DNA-SH, MCH and improve the interfacial conductivity (Zhang et al., 2019; Zhou et al., 2017). Then, the sandwich-type immune process was carried out in a tube. When the target NSE was present, it can be captured by Ab_1-MBs firstly. After that, Ab_2-PtCu immunoprobes were combined with NSE/Ab_1-MBs to form the sandwiched immunocomplexes (Ab_2-PtCu/NSE/Ab_1-MBs) via antigen-antibody specific recognition. With the addition of H_2O_2 and iodide, the nanoprobes as catalyst accelerated the oxidation of iodide to iodine and consumed the amount of iodide in the tube. Subsequently, in the presence of H_2O_2, the iodide of residual solution after immunoreaction further catalyzed the oxidation of thiol substances (RSH) to yield disulfide substances (RSSH), resulting in DNA-SH and MCH on the electrode surface to form disulfide substances and detach from the electrode surface after washing with PBS (pH = 7.4). By virtue of the poor conductivity of DNA and MCH, the decline of DNA-SH and MCH can increase electron transfer between sensing interface and $[Fe(CN)_6]^{3-/4-}$ by lowering the interface resistance. In addition, it was worth noting that MCH can be considered as the enhancer of -SH amount. And the current differences

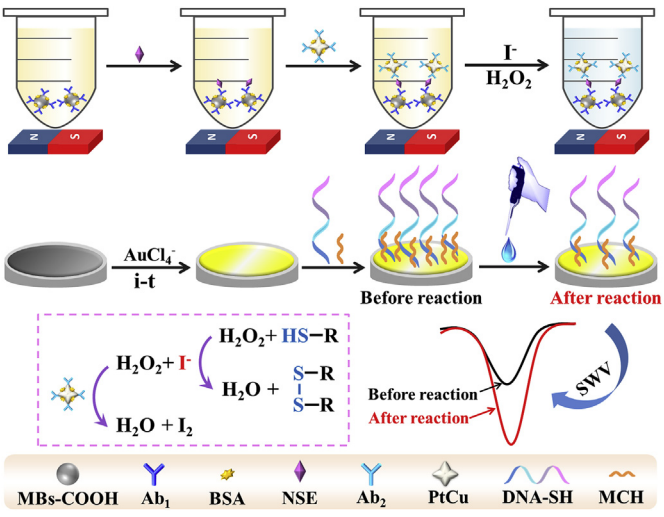

Scheme 1. Schematic diagram of sandwich-type immune process and electrochemical detection for NSE.

(ΔI = I_b − I_a, where I_a and I_b are the current peak of sensing interface before and after the -SH oxidation reaction) without (Fig. S1A, ΔI_1 = 14.49 μA) and with (Fig. S1B, ΔI_2 = 19.81 μA) MCH were shown in Fig. S1, indicating that the introduction of MCH increased the current difference of sensing interface. By means of PtCu nanoprobe-initiated cascade reaction and iodide-responsive sensing interface, different concentrations of target analyte were corresponding to different increase of current signals so as to achieve the sensitive detection of NSE.

3.2. Characterization of PtCu nanoparticles

The morphology of as-prepared PtCu nanoparticles was characterized by HRTEM. As indicated in Fig. 1A, the average size of PtCu nanoparticles was around 40 nm. To further illuminate by HRTEM, Fig. 1B displayed many visible lattice fringes. The lattice fringes were marked in Fig. 1a-b and calculated to be 0.221 nm, which was between the distance of (1 1 1) planes of pure fcc Cu (0.209 nm) and Pt (0.226 nm) (Du et al., 2018), indicating the successful preparation of PtCu alloy (Guo et al., 2017). In addition, to characterize the element composition, the energy dispersive spectroscopy (EDS) spectrum of PtCu nanoparticles was shown in Fig. 1C. The weight ratio and atomic ratio of Cu/Pt were about 33.02/66.08 and 60.22/39.78, respectively.

X-ray photoelectron spectroscopy (XPS) illustrated the element composition and chemical state of PtCu nanoparticles in Fig. S2. The high-resolution XPS spectrum of Cu 2p was displayed in Fig. 2A, which showed the characteristic peaks at 951.68 eV and 931.88 eV in accordance with Cu $2p_{1/2}$ and Cu $2p_{3/2}$ of Cu^0 (Cu^+). Also, the characteristic peaks at 954.15 eV and 934.28 eV were ascribed to Cu $2p_{1/2}$ and Cu $2p_{3/2}$ of Cu^{2+} because of the partial oxidation of Cu atoms in the atmosphere (Fu et al., 2016; Gong et al., 2014). Furthermore, two peaks were also observed at 941.01 eV and 943.27 eV in accordance with the satellite peaks of CuO (Li et al., 2019). In addition, as described in Fig. 2B, two strong characteristic peaks at 74.33 eV and 70.98 eV was shown in the high-resolution XPS spectrum of Pt 4f, which were attributed to Pt $4f_{5/2}$ and Pt $4f_{7/2}$ of Pt^0. Also, two relatively weak peaks at 76.51 eV and 72.03 eV were associated to Pt $4f_{5/2}$ and Pt $4f_{7/2}$ of Pt^{2+} from $Pt(OH)_2$ or PtO (Zhang et al., 2018b), indicating Pt^0 was the predominant chemical state of Pt element on the catalyst surface (Huang et al., 2018; Niu et al., 2019). Seen from these results of XPS, we verified the reduction of Cu^{2+} and Pt^{2+} and the successful synthesis of PtCu nanoparticles.

UV–vis spectrum was presented to prove the catalytic property of PtCu nanoparticles in Fig. S3. Compared with iodide + H_2O_2 (curve a), the group of iodide + H_2O_2 + PtCu (curve b) showed weaker absorption peak at 225 nm and stronger absorption peak at 282 nm, which respectively corresponded to the characteristic absorption peak of iodide and iodine, indicating the catalytic property of PtCu nanoparticles towards the oxidation of iodide to iodine.

3.3. Characterization of electrochemical sensing interface

The stepwise modification process of sensing interface was characterized by cyclic voltammetry (CV) measurement (Fig. 3A). Owing to good conductivity, the Au nanoparticles modified electrode (curve b) showed higher current response when comparing with bare electrode (curve a). Furthermore, the SEM image and EDS analysis of Au nanoparticles modified electrode were respectively shown in Fig. S4A and Fig. S4B. After the incubation of DNA-SH (curve c), the current signal decreased obviously due to poor conductivity of DNA and electrostatic repulsion between electronegative DNA and redox species $[Fe(CN)_6]^{4-/3-}$. Subsequently, MCH caused a further decrease in current signal (curve d). After the reaction of DNA-SH and MCH with iodide and H_2O_2 (curve e), the current signal increased owing to the decline of DNA-SH and MCH amount and the increase of electron transfer between the sensing interface and $[Fe(CN)_6]^{3-/4-}$.

Electrochemical impedance spectroscopy (EIS) measurement

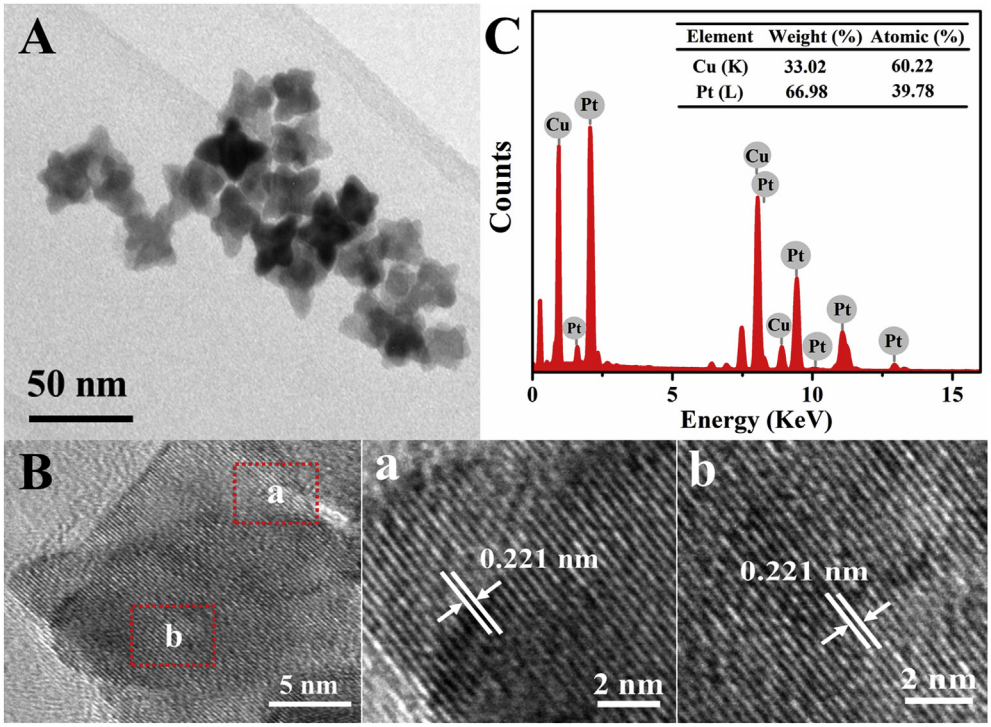

Fig. 1. HRTEM images of as-prepared PtCu nanoparticles (A) and an individual part of PtCu nanoparticle (B). (a–b) HRTEM images taken from the red marked regions in B. EDS spectrum of PtCu nanoparticles (C). Inset in C shows the weight ratio and atomic ratio of Cu/Pt. (For interpretation of the references to colour in this figure legend, the reader is referred to the Web version of this article.)

(Fig. 3B) was also utilized to monitor the modification procedure of sensing interface. In Nyquist plot, the semicircle diameter was in accordance with the charge transfer resistance. Seen from Fig. 3B, compared to bare GCE (curve a), the Au nanoparticles modified GCE (curve b) exhibited a smaller semicircle, indicating Au nanoparticles enhanced the conductivity of sensing interface. Then, the interface resistance increased successively after the modification of DNA-SH (curve c) and MCH (curve d). After the reaction with iodide and H_2O_2 (curve e), DNA and MCH with poor conductivity was detached from the electrode surface by washing with PBS (pH = 7.4), which caused apparent decrease of interfacial resistance. These results of CV and EIS measurement were consistent, suggesting successful construction of electrochemical sensing interface.

3.4. Verification the changes of DNA amount on electrodes

The changes in the amount of DNA on the sensing interface were quantified by chronocoulometry (CC) method (Liu et al., 2015; Steel et al., 1998). Herein, the amount of DNA was quantitatively determined by utilizing the electrostatic attraction between RuHex and nucleotide phosphate backbone of DNA. The related principle, process and equations were detailedly expatiated in the published literature (Steel et al., 1998). Specifically, the typical chronocoulometric response for RuHex was provided in Fig. S5. Before the -SH oxidation reaction, the amount of DNA-SH was calculated to be 3.16×10^{11} molecules (Fig. S5A). While, after the -SH oxidation reaction, the amount of DNA-SH was calculated to be 5.84×10^{10} molecules (Fig. S5B), indicating the significant decrease of DNA-SH on the electrode surface. In addition, the obvious signal differences can be observed by CV (Fig. 4A), SWV (Fig. 4B) and EIS measurements (Fig. 4C) after the oxidation of -SH, which further demonstrated the decrease in the amount of DNA-SH and the feasibility of this strategy.

3.5. Optimization of experimental parameters

The experimental conditions including the concentration of DNA-SH, the incubation time of Ab_2-PtCu nanoprobes and the reaction time of -SH oxidation were investigated to attain the optimal analytical performance. Because DNA-SH acted as the main reactant in the -SH oxidation reaction, the concentration of DNA-SH influenced the analytical performance of biosensor significantly. As presented in Fig. S6A, current values lowered with DNA-SH concentration from 100 nM to

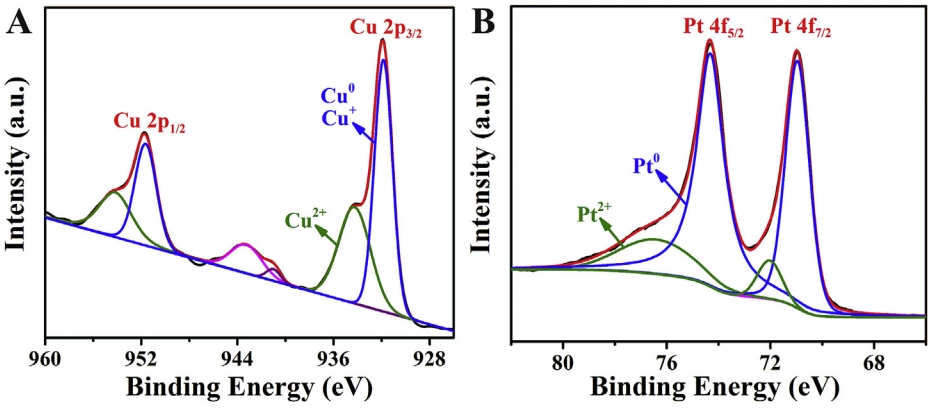

Fig. 2. The high-resolution XPS spectra of Cu 2p (A) and Pt 4f (B).

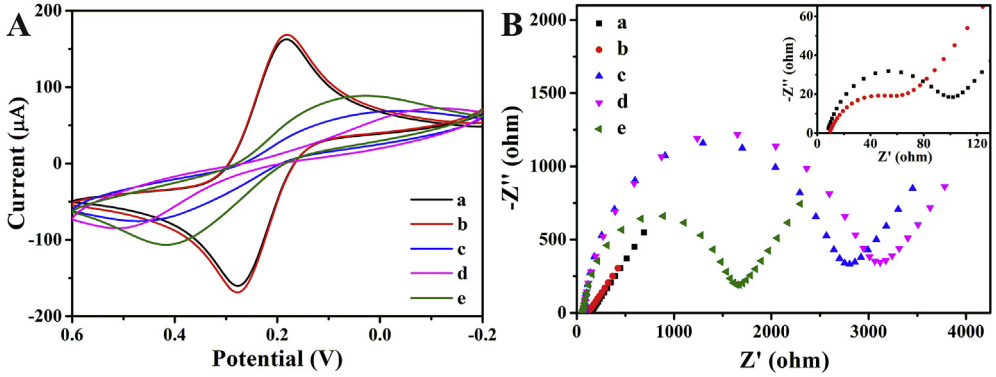

Fig. 3. CV (A) and EIS (B) of different modified electrodes in 5 mM $[Fe(CN)_6]^{3-/4-}$ containing 0.1 M KCl: GCE (a), Au/GCE (b), DNA-SH/Au/GCE (c), MCH/DNA-SH/Au/GCE (d) and after the reaction of DNA-SH with iodide and H_2O_2 (e). Inset in B shows the magnified view of EIS of GCE and Au/GCE.

1 μM and remained almost stable after 1 μM, which were caused by the high resistance of DNA and electrostatic repulsion of DNA and $[Fe(CN)_6]^{4-/3-}$. Thus, to maximize the amount of reactant for -SH oxidation reaction, 1 μM was selected as the optimal DNA-SH concentration. Also, the incubation time of Ab_2-PtCu nanoprobes was investigated in Fig. S6B. The current values decreased gradually with incubation time from 20 to 50 min until it remained constant, suggesting that 50 min as the optimal incubation time was chosen for nanoprobes. Furthermore, the reaction time of -SH oxidation also affected the performance of the immunosensor. Seen from Fig. S6C, the current values increased with reaction time from 20 to 40 min then reached a plateau. We therefore selected 40 min as the optimum reaction time of -SH oxidation.

3.6. Analytical performance for NSE detection

The SWV measurement was applied to measure a series of NSE standard solutions under optimal conditions. The current values decreased gradually with the increase of NSE concentration from 0.0001 to 100 ng mL^{-1} in Fig. 5A. Then as is shown in Fig. 5B, current values of SWV and logarithm values of NSE concentration presented a good linear relationship. The corresponding linear equation was $I = 5.85\ lgC - 57.87$ ($R^2 = 0.9989$), which can calculate the detection limit of 52.14 fg mL^{-1} for NSE. Compared with analytical performance for NSE detection in previous references (Table S2), this immunosenor showed wider detection range and lower detection limit.

3.7. Selectivity, repeatability and stability

To investigate the selectivity of this biosensor, NSE (0.1 ng mL^{-1}) with different interferences such as IgG (10 ng mL^{-1}), PSA (10 ng mL^{-1}), CEA (10 ng mL^{-1}), CA199 (10 U mL^{-1}) and CA242 (10 U mL^{-1}) was detected by the designed immunosensor. As indicated in Fig. S7, the current values were almost identical between NSE containing different distractions and that of only NSE, suggesting the superior specificity for NSE. Five independent electrodes under the same conditions were employed to analyze the repeatability of the biosensor (Fig. S8A). And relative standard deviation (RSD) of five electrodes was 2.37%, which indicated the acceptable reproducibility. In addition, the stability was also evaluated by storing modified electrodes in a refrigerator for four weeks at 4 °C (Fig. S8B). After four weeks, the current still kept 94.8% of initial current value and the RSD was below 5%, revealing the high stability of this biosensor.

3.8. Human serum samples analysis

To demonstrate the reliability of this immunosensor, contrast experiments were determined by the biosensor and chemiluminescence immunoassay (CMIA) in human serum samples. As presented in Table S3, the RSD was in the range of 0.40%–1.21% and relative error was in the range of −3.11%–6.29%, which illustrated the acceptable reliability of immunosensor in clinical application.

4. Conclusion

In summary, an improved electrochemical biosensor was proposed on the basis of PtCu nanoprobe-initiated cascade reaction and iodide-responsive sensing interface for NSE detection. Noteworthy, the strategy was implemented by transferring the immunoreaction from electrode surface to tube so that the interface resistance was lowered significantly and the current differences caused by target were improved notably. Furthermore, making use of the catalytic activities of PtCu nanoparticles and iodide, PtCu nanoprobe-initiated cascade reaction greatly enhanced the sensitivity of immunosensor. And it was important that this method effectively simplified the operation steps on electrode surface to reduce the non-specific adsorption and the contamination of sensing interface, thereby improving the analysis performance of electrochemical biosensor. Given the advantages of this sensing interface, wide detection range and ultralow detection limit can be obtained by the designed biosensor with good selectivity, stability and repeatability. Therefore, this improved electrochemical

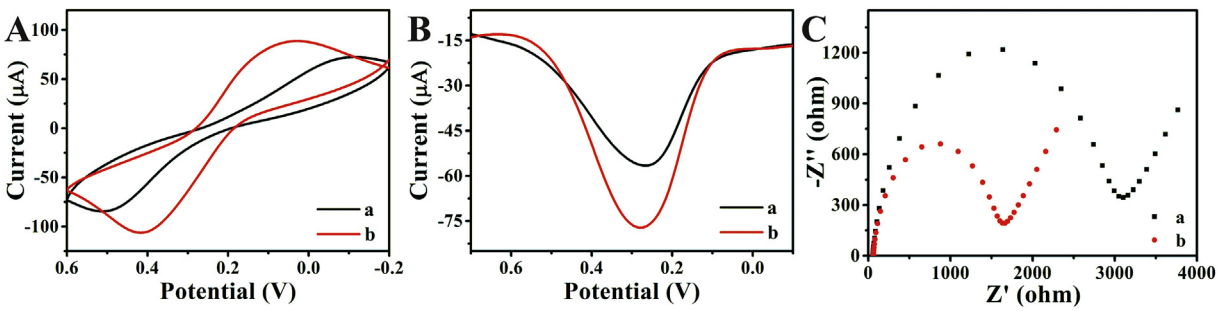

Fig. 4. CV (A), SWV (B) and EIS (C) measurements before (a) and after (b) the oxidation reaction of -SH.

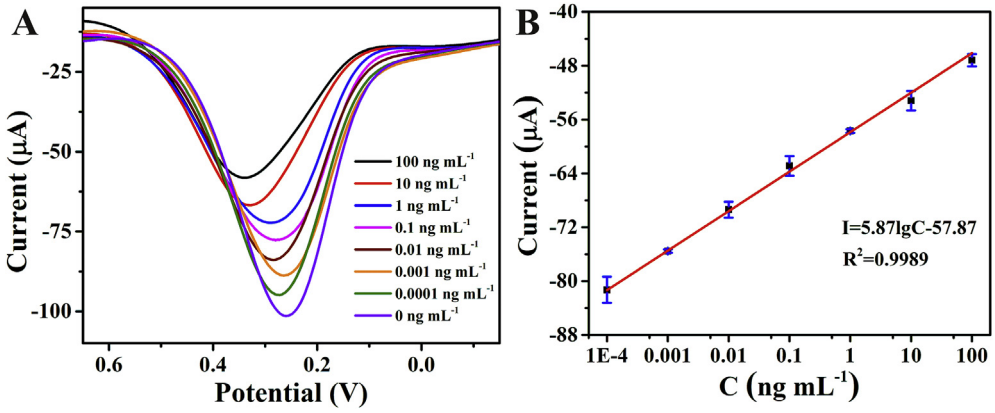

Fig. 5. (A) SWV responses of the improved electrochemical biosensor toward different NSE concentrations from blank to 100 ng mL^{-1} in 0.01 M PBS (pH = 7.4) containing 5 mM $[Fe(CN)_6]^{3-/4-}$. (B) Calibration curve between current values of SWV and the different concentrations of NSE.

immunosenosor provided a promising means of other biomarkers determination. Moreover, if the nanoprobes could possess higher catalytic activity, the analytical performance of the sensing interface can be further improved and the proposed immunosensor can offer a more sensitive approach to diagnose cancer in clinical applications.

CRediT authorship contribution statement

Chi Zhang: Writing - original draft. **Zhanfang Ma:** Supervision.

Declaration of competing interest

The authors declare that they have no known competing financial interests or personal relationships that could have appeared to influence the work reported in this paper.

Acknowledgements

This research was financed by grants from the National Natural Science Foundation of China (21673143), Natural Science Foundation of Beijing Municipality (2172016), and Capacity Building for Sci-Tech Innovation-Fundamental Scientific Research Funds (19530050179).

Appendix A. Supplementary data

Supplementary data to this article can be found online at https://doi.org/10.1016/j.bios.2019.111612.

References

Carney, D.N., Ihde, D.C., Cohen, M.H., Marangos, P.J., Bunn, P.A., Minna, J.D., Gazdar, A.F., 1982. Lancet 1, 583–585.
Du, Y., Ni, K., Zhai, Q., Yun, Y., Xu, Y., Sheng, H., Zhu, Y., Zhu, M., 2018. Appl. Catal., A 557, 72–78.
Eisenhauer, E.A., Therasse, P., Bogaerts, J., Schwartz, L.H., Sargent, D., Ford, R., Dancey, J., Arbuck, S., Gwyther, S., Mooney, M., Rubinstein, L., Shankar, L., Dodd, L., Kaplan, R., Lacombe, D., Verweij, J., 2009. Eur. J. Cancer 45, 228–247.
Fan, G.C., Han, L., Zhu, H., Zhang, J.R., Zhu, J.J., 2014. Anal. Chem. 86, 12398–12405.
Fu, G., Liu, H., You, N., Wu, J., Sun, D., Xu, L., Tang, Y., Chen, Y., 2016. Nano Res 9, 755–765.
Gao, X., Zheng, P., Kasani, S., Wu, S., Yang, F., Lewis, S., Nayeem, S., Engler-Chiurazzi, E.B., Wigginton, J.G., Simpkins, J.W., Wu, N., 2017. Anal. Chem. 89, 10104–10110.
Gong, M., Fu, G., Chen, Y., Tang, Y., Lu, T., 2014. ACS Appl. Mater. Interfaces 6, 7301–7308.
Guo, L., Huang, L.B., Jiang, W.J., Wei, Z.D., Wan, L.J., Hu, J.S., 2017. J. Mater. Chem. A 5, 9014–9021.
Han, J., Zhuo, Y., Chai, Y.Q., Yuan, Y.L., Yuan, R., 2012. Biosens. Bioelectron. 31, 399–405.
Hou, L., Gao, Z., Xu, M., Cao, X., Wu, X., Chen, G., Tang, D., 2014. Biosens. Bioelectron. 54, 365–371.
Huang, X.Y., Wang, A.J., Zhang, L., Fang, K.M., Wu, L.J., Feng, J.J., 2018. J. Colloid Interface Sci. 531, 578–584.
Ko, H., Lee, J., Kim, Y., Lee, B., Jung, C.H., Choi, J.H., Kwon, O.S., Shin, K., 2014. Adv. Mater. 26, 2335–2340.
Li, F., Feng, J., Gao, Z., Shi, L., Wu, D., Du, B., Wei, Q., 2019. ACS Appl. Mater. Interfaces 11, 8945–8953.
Li, H., Xiao, Q., Lv, J., Lei, Q., Huang, Y., 2017. Anal. Biochem. 531, 48–55.
Li, J., Li, X., Feng, W., Huang, L., Zhao, Y., Hu, Y., Cai, K., 2018. Mater. Lett. 229, 193–197.
Liang, X.Y., Han, H.L., Ma, Z.F., 2019. Sens. Actuators, B 290, 625–630.
Liu, R., Yang, Z., Guo, Q., Zhao, J., Ma, J., Kang, Q., Tang, Y., Xue, Y., Lou, X., He, M., 2015. Electrochim. Acta 182, 516–523.
Niu, H.J., Chen, H.Y., Wen, G.L., Feng, J.J., Zhang, Q.L., Wang, A.J., 2019. J. Colloid Interface Sci. 539, 525–532.
Ren, R., Cai, G., Yu, Z., Zeng, Y., Tang, D., 2018. Anal. Chem. 90, 11099–11105.
Ren, X., Ma, H., Zhang, T., Zhang, Y., Yan, T., Du, B., Wei, Q., 2017. ACS Appl. Mater. Interfaces 9, 37637–37644.
Riedel, T., Riedelova-Reicheltova, Z., Majek, P., Rodriguez-Emmenegger, C., Houska, M., Dyr, J.E., Brynda, E., 2013. Langmuir 29, 3388–3397.
Steel, A.B., Herne, T.M., Tarlov, M.J., 1998. Anal. Chem. 70, 4670–4677.
Wang, G., Xu, Q., Liu, L., Su, X., Lin, J., Xu, G., Luo, X., 2017. ACS Appl. Mater. Interfaces 9, 31153–31160.
Wang, H.Q., Ma, Z.F., 2019. Biosens. Bioelectron. 132, 265–270.
Wang, L., 2017. Sensors (Basel) 17, 2420.
Wang, X., Wang, Y., Ye, X., Wu, T., Deng, H., Wu, P., Li, C., 2018. Biosens. Bioelectron. 99, 34–39.
Wei, Y., Li, X., Sun, X., Ma, H., Zhang, Y., Wei, Q., 2017. Biosens. Bioelectron. 94, 141–147.
Yang, G., Xiao, Z., Tang, C., Deng, Y., Huang, H., He, Z., 2019. Biosens. Bioelectron. 141, 111416.
Yang, L., Zhu, W., Ren, X., Khan, M.S., Zhang, Y., Du, B., Wei, Q., 2017. Biosens. Bioelectron. 91, 842–848.
Yin, S., Ma, Z.F., 2019. Biosens. Bioelectron. 140, 111355.
Yin, S., Zhao, L.H., Ma, Z.F., 2018. Anal. Bioanal. Chem. 410, 1279–1286.
Zhang, C., Zhang, D.S., Ma, Z.F., Han, H.L., 2019. Biosens. Bioelectron. 137, 1–7.
Zhang, D.S., Li, W.X., Ma, Z.F., 2018a. Biosens. Bioelectron. 109, 171–176.
Zhang, X.F., Wang, A.J., Zhang, L., Yuan, J., Li, Z., Feng, J.J., 2018b. ACS Appl. Mater. Interfaces 1, 5054–5061.
Zhao, J.C., Shu, D., Ma, Z.F., 2019. Biosens. Bioelectron. 127, 161–166.
Zhao, L.H., Ma, Z.F., 2017. Sens. Actuators, B 241, 849–854.
Zheng, Y., Ma, Z.F., 2019. Biosens. Bioelectron. 129, 42–49.
Zhou, X., Guo, S., Gao, J., Zhao, J., Xue, S., Xu, W., 2017. Biosens. Bioelectron. 98, 83–90.
Zhou, X., Qian, X., Tan, X., Ran, X., Li, Z., Huang, Z., Yang, L., Xie, X., 2019. Anal. Chim. Acta 1068, 18–27.